

# Off-shell effects in Higgs decays to heavy gauge bosons and signal-background interference in Higgs decays to photons at a linear collider

Stefan Liebler

*DESY, Notkestraße 85,  
22607 Hamburg, Germany*

## Abstract

We discuss off-shell contributions in Higgs decays to heavy gauge bosons  $H \rightarrow VV^{(*)}$  with  $V \in \{Z, W\}$  for a standard model (SM) Higgs boson for both dominant production processes  $e^+e^- \rightarrow ZH \rightarrow ZVV^{(*)}$  and  $e^+e^- \rightarrow \nu\bar{\nu}H \rightarrow \nu\bar{\nu}VV^{(*)}$  at a (linear)  $e^+e^-$  collider. Dependent on the centre-of-mass energy off-shell effects are sizable and important for the understanding of the electroweak symmetry breaking mechanism. Moreover we shortly investigate the effects of the signal-background interference in  $H \rightarrow \gamma\gamma$  decays for the Higgsstrahlung initiated process  $e^+e^- \rightarrow Z\gamma\gamma$ , where we report a similar shift in the invariant mass peak of the two photons as found for the LHC. For both effects we discuss the sensitivity to the total Higgs width.

# 1 Introduction

After the discovery of a scalar boson at the Large Hadron Collider (LHC) [1,2] a major task of particle physics is the precise determination of its couplings and its mass in order to reveal the mechanism of electroweak symmetry breaking and to determine whether it is the standard model (SM) Higgs boson. Recently two interesting effects to test the underlying nature were discussed at the LHC, a measurement of off-shell Higgs boson decays into heavy gauge bosons as well as a shift in the invariant mass peak of the two photons in Higgs boson decays to photons, the latter due to signal-background interference terms. Both – under certain theoretical assumptions – are sensitive to the total Higgs width. It is timely to discuss the two effects for a (linear)  $e^+e^-$  collider, not only for what concerns constraints on the Higgs width, but also to elaborate on the phenomenological consequences of the effects. We subsequently first discuss off-shell Higgs boson decays to heavy gauge bosons and afterwards the signal-background interference for Higgs boson decays to photons.

## 2 Off-shell effects in $H \rightarrow VV^{(*)}$

In this section we want to discuss off-shell effects in Higgs boson decays  $H \rightarrow VV^{(*)}$  with  $V \in \{Z, W\}$  at an  $e^+e^-$  collider, where we focus on both production processes  $e^+e^- \rightarrow ZH$  and  $e^+e^- \rightarrow \nu\bar{\nu}H$ . For a more detailed discussion we refer to Ref. [3], where also the relation between the mass and the total width of the Higgs boson and the complex pole of the propagator is presented. In accordance to the LHC Higgs cross section working group (LHC-HXSWG) [4] we choose the total width  $\Gamma_H^{\text{SM}} = 4.07 \cdot 10^{-3} \text{ GeV}$  for a SM Higgs boson with mass  $m_H = 125 \text{ GeV}$  in the subsequent discussion.

Following Refs. [5] for the case of the LHC, it is well established that the kinematic region, where the invariant mass of the two gauge bosons  $m_{VV}$  in  $H \rightarrow VV^{(*)}$  exceeds twice the gauge boson masses  $2m_V$ , contributes a sizable fraction of several percent to the total inclusive cross section  $gg \rightarrow H \rightarrow VV^{(*)}$ . A combination of on- and off-shell effects was identified to allow to constrain the total Higgs width [6], however under strong theoretical assumptions [7]. Obtained experimental bounds from the CMS and the ATLAS collaboration can be found in Refs. [8], where apart from the gluon fusion production process a similar effect for vector-boson fusion was used. Recently a discussion of the off-shell effects for an  $e^+e^-$  collider was carried out in Ref. [3] with many analogies to the LHC discussion. Subsequently we shortly summarize the findings: The large off-shell contribution to the total process  $e^+e^- \rightarrow ZH$  and  $e^+e^- \rightarrow \nu\bar{\nu}H$  with the Higgs boson decays  $H \rightarrow WW^{(*)}$  and  $H \rightarrow ZZ^{(*)}$  (see Fig. 1 for Feynman diagrams) can be understood as inadequacy of the zero-width approximation (ZWA) in the description of the process. Using it for the production and decay part of the process one can define [5]

$$\left( \frac{d\sigma_{\text{ZWA}}^{ZVV}}{dm_{VV}} \right) = \sigma^{ZH}(m_H) \frac{2m_{VV}}{(m_{VV}^2 - m_H^2)^2 + (m_H\Gamma_H)^2} \frac{m_H\Gamma_{H \rightarrow VV}(m_H)}{\pi}, \quad (1)$$

which we later compare to the description given by the off-shell production cross section according to [3, 5]

$$\left( \frac{d\sigma_{\text{off}}^{ZVV}}{dm_{VV}} \right) = \sigma^{ZH}(m_{VV}) \frac{2m_{VV}}{(m_{VV}^2 - m_H^2)^2 + (m_H\Gamma_H)^2} \frac{m_{VV}\Gamma_{H \rightarrow VV}(m_{VV})}{\pi}. \quad (2)$$

For two processes additional comments are on order: For  $e^+e^- \rightarrow \nu\bar{\nu}W^+W^-$  apart from the contribution which involves an  $s$ -channel Higgs boson in the off-shell region corresponding

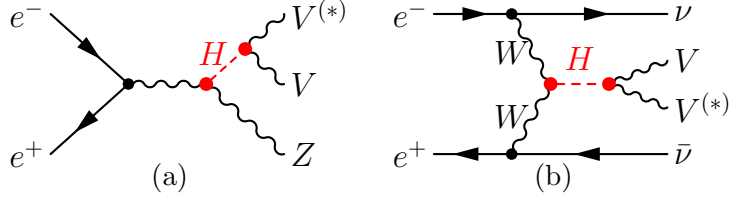


Figure 1: Feynman diagrams for the two dominant production processes (a)  $e^+e^- \rightarrow ZH$  followed by  $H \rightarrow VV^{(*)}$  and (b)  $e^+e^- \rightarrow \nu\bar{\nu}H$  followed by  $H \rightarrow VV^{(*)}$ .

to the approximation given by Eq.(2), also the  $t$ -channel Higgs boson exchange between the gauge bosons is of relevance and thus added to the Higgs boson induced contributions. Secondly for  $e^+e^- \rightarrow ZH \rightarrow ZZZ$  it is a priori unclear which two out of three  $Z$  bosons originate from an intermediate Higgs boson. We thus also average over the three possible invariant mass combinations  $m_{VV}$ , which however induces on-shell Higgs boson events to contribute in the off-shell region  $m_{ZZ} > 2m_Z$ . For what concerns the gauge invariance of our discussion, the inclusion of higher order contributions or initial-state radiation we refer to Ref. [3].

We show the differential cross sections  $d\sigma/dm_{ZZ}$  for  $e^+e^- \rightarrow ZH$  and  $e^+e^- \rightarrow \nu\bar{\nu}H$  followed by  $H \rightarrow ZZ^{(*)}$  for different centre-of-mass (cms) energies  $\sqrt{s} = 250, 350, 500$  GeV and 1 TeV, but a fixed polarisation of the initial state being  $\text{Pol}(e^+, e^-) = (0.3, -0.8)$  in Fig. 2. Our results are obtained using `FeynArts`, `FormCalc` [9] and `MadGraph5_aMC@NLO` [10]. As indicated for  $e^+e^- \rightarrow ZZZ$  we average over the three possible invariant mass combinations of  $ZZ$  pairs presented by the red, dot-dashed curve, but also present the result obtained by the usage of Eq.(2). Similarly, we show the differential cross sections for both production processes followed by  $H \rightarrow WW^{(*)}$  in Fig. 3, where we add the red, dot-dashed curve including the  $t$ -channel Higgs boson induced contributions. In both Figs. 2 and 3 we also show the total differential cross section for the specific final state as blue curve, thus including the contributions from background diagrams with the same final state. For a detailed discussion of the background we refer to Ref. [3].

In order to quantify the relative importance of the off-shell signal contributions we define

$$\Delta_{\text{off}}^{ZVV} = \frac{\sigma_{\text{off}}^{ZVV}(130\text{GeV}, \sqrt{s} - m_Z)}{\sigma_{\text{off}}^{ZVV}} \quad \text{and} \quad \Delta_{\text{off}}^{\nu\bar{\nu}VV} = \frac{\sigma_{\text{off}}^{\nu\bar{\nu}VV}(130\text{GeV}, \sqrt{s})}{\sigma_{\text{off}}^{\nu\bar{\nu}VV}} \quad (3)$$

with the inclusive cross section for a lower and upper bound of masses  $m_{VV}$

$$\sigma_X(m_{VV}^d, m_{VV}^u) = \int_{m_{VV}^d}^{m_{VV}^u} dm_{VV} \left( \frac{d\sigma_X}{dm_{VV}} \right) \quad . \quad (4)$$

and  $\sigma_{\text{off}}^{ZVV} = \sigma_{\text{off}}^{ZVV}(0, \sqrt{s} - m_Z)$  as well as  $\sigma_{\text{off}}^{\nu\bar{\nu}VV} = \sigma_{\text{off}}^{\nu\bar{\nu}VV}(0, \sqrt{s})$ .  $\Delta_{\text{off}}$  is hardly sensitive to the boundary value between on- and off-shell contributions at 130 GeV. We present the polarisation independent values  $\Delta_{\text{off}}$  as a function of the cms energy in Tab. 1. As it can be seen from Tab. 1 the off-shell contributions reach  $\mathcal{O}(10\%)$  for large cms energies. Naturally, the on-shell Higgs cross section is much dependent on the precise numerical value of the Higgs mass, whereas the off-shell contributions are insensitive to the latter value. In extended Higgs sectors the off-shell contributions of the light SM-like Higgs can interfere with on-shell contributions of a heavy Higgs, as it was demonstrated for a linear collider in the context of a 2-Higgs-doublet model in Ref. [3]. Similar findings were reported for the LHC in Refs. [11].

The  $Z$  recoil mass measurement is the first step of a unique method to obtain the Higgs width at a linear collider, often named  $Z$  recoil method [12]. It is only hardly affected by

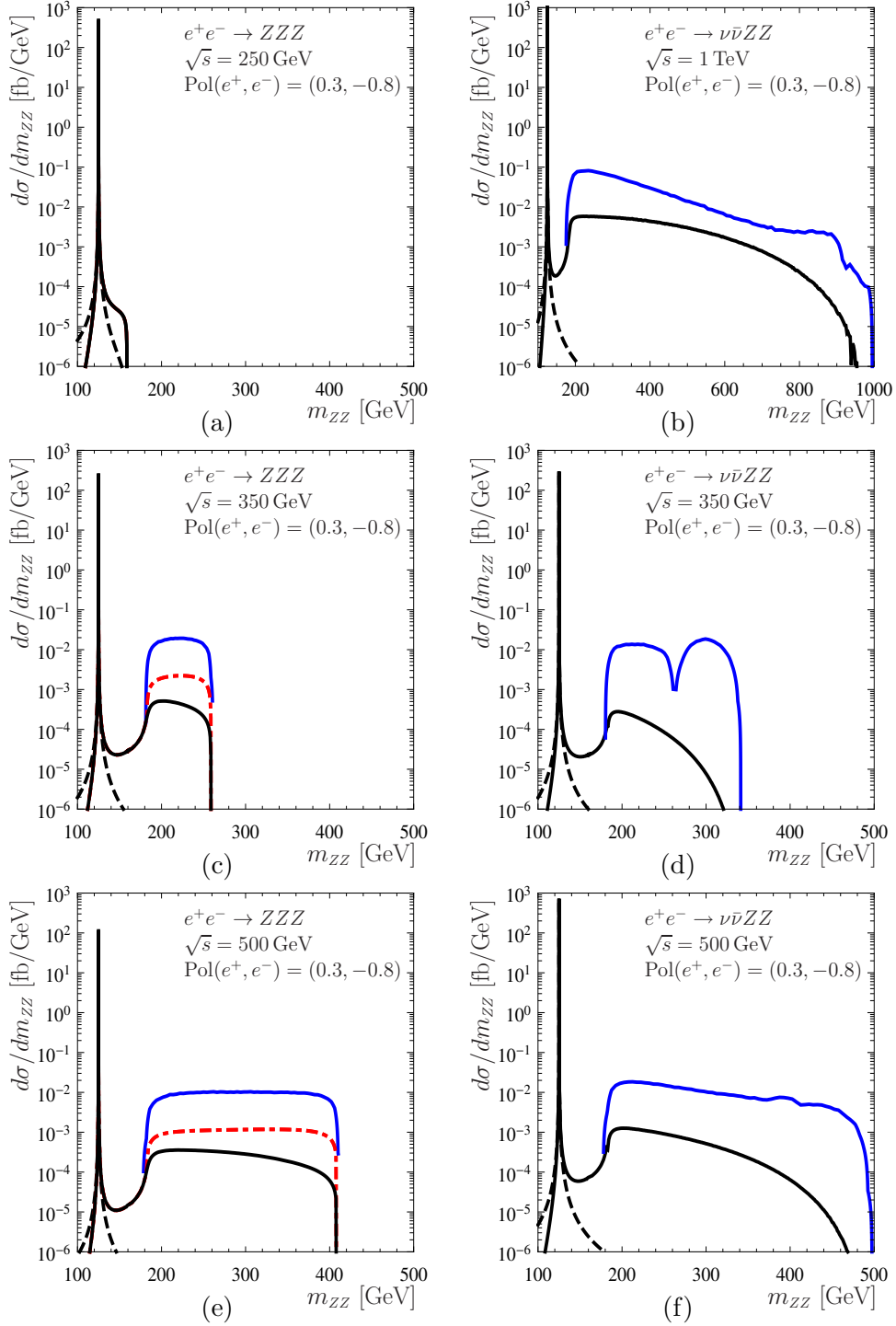


Figure 2:  $d\sigma/dm_{ZZ}$  in fb/GeV as a function of  $m_{ZZ}$  in GeV according to Eq. (1) (ZWA) (black, dashed) and Eq. (2) (black, solid) for (a,c,e)  $e^+e^- \rightarrow ZH \rightarrow ZZZ$  for cms energies  $\sqrt{s} = 250, 350, 500$  GeV (top to bottom) and (b,d,f)  $e^+e^- \rightarrow \nu\bar{\nu}H \rightarrow \nu\bar{\nu}ZZ$  for cms energies  $\sqrt{s} = 1000, 350, 500$  GeV (top to bottom) with a fixed polarisation  $\text{Pol}(e^+, e^-) = (0.3, -0.8)$ . The calculation of  $e^+e^- \rightarrow ZH \rightarrow ZZZ$  with an average over the  $ZZ$  pairs is presented by the red, dot-dashed curve. The complete calculation  $e^+e^- \rightarrow ZZZ/\nu\bar{\nu}ZZ$  is depicted by the blue curve.

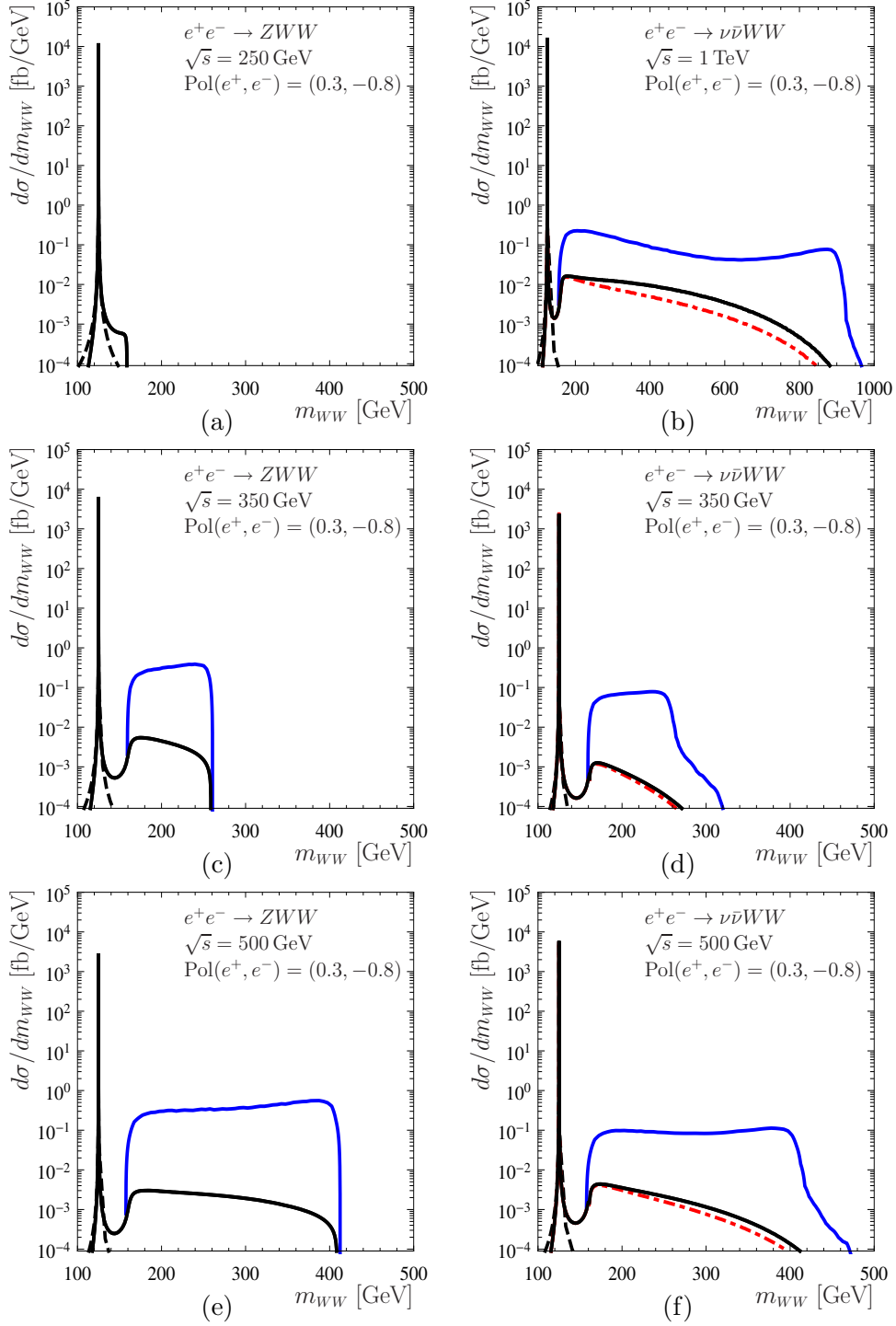


Figure 3:  $d\sigma/dm_{WW}$  in fb/GeV as a function of  $m_{WW}$  in GeV according to Eq. (1) (ZWA) (black, dashed) and Eq. (2) (black, solid) for (a,c,e)  $e^+e^- \rightarrow ZH \rightarrow ZWW$  for cms energies  $\sqrt{s} = 250, 350, 500$  GeV (top to bottom) and (b,d,f)  $e^+e^- \rightarrow \nu\bar{\nu}H \rightarrow \nu\bar{\nu}WW$  for cms energies  $\sqrt{s} = 1000, 350, 500$  GeV (top to bottom) with a fixed polarisation  $\text{Pol}(e^+, e^-) = (0.3, -0.8)$ . We add both  $s$ - and  $t$ -channel Higgs induced contributions for  $e^+e^- \rightarrow \nu\bar{\nu}WW$  as red, dot-dashed curve. The complete differential cross section including background diagrams yielding the same final state is depicted as blue curve.

$\sqrt{s}$	$\sigma_{\text{off}}^{ZZZ}$	$\Delta_{\text{off}}^{ZZZ}$	$\sigma_{\text{off}}^{\nu\bar{\nu}ZZ}$	$\Delta_{\text{off}}^{\nu\bar{\nu}ZZ}$
250 GeV	(3.12)3.12 fb	(0.03)0.03 %	0.490 fb	0.12 %
300 GeV	(2.40)2.36 fb	(1.83)0.46 %	1.12 fb	0.40 %
350 GeV	(1.82)1.71 fb	(7.77)1.82 %	1.91 fb	0.88 %
500 GeV	(0.981)0.802 fb	(24.1)7.20 %	4.78 fb	2.96 %
1 TeV	(0.341)0.242 fb	(50.9)30.9 %	15.0 fb	13.0 %
$\sqrt{s}$	$\sigma_{\text{off}}^{ZWW}$	$\Delta_{\text{off}}^{ZWW}$	$\sigma_{\text{off}}^{\nu\bar{\nu}WW}$	$\Delta_{\text{off}}^{\nu\bar{\nu}WW}$
250 GeV	76.3 fb	0.03 %	(3.99)3.98 fb	(0.12)0.13 %
300 GeV	57.7 fb	0.42 %	(9.08)9.07 fb	(0.26)0.29 %
350 GeV	41.4 fb	0.92 %	(15.5)15.5 fb	(0.43)0.49 %
500 GeV	18.6 fb	2.61 %	(38.1)38.2 fb	(0.96)1.21 %
1 TeV	4.58 fb	11.0 %	(108.9)110.8 fb	(2.78)4.45 %

Table 1: Inclusive cross sections  $\sigma_{\text{off}}$  for  $e^+e^- \rightarrow ZH \rightarrow ZVV$  and for  $e^+e^- \rightarrow \nu\bar{\nu}H \rightarrow \nu\bar{\nu}VV$  for a polarisation of  $\text{Pol}(e^+, e^-) = (0.3, -0.8)$  and relative size of the off-shell contributions  $\Delta_{\text{off}}$  in %. The results averaging over the  $ZZ$  pairs for  $e^+e^- \rightarrow ZZZ$  and taking into account the  $t$ -channel Higgs contribution for  $e^+e^- \rightarrow \nu\bar{\nu}WW$  are added in brackets.

off-shell contributions to Higgs boson decays into heavy gauge bosons at low cms energies  $\sqrt{s} = 250 - 350$  GeV [3]. Contrary off-shell contributions provide their own method of constraining the Higgs width, when combining them with the on-shell measurement of Higgs boson decays, however we pointed to the strong theoretical limitations. To demonstrate its limitations compared to the  $Z$  recoil method we simulate the process  $e^+e^- \rightarrow \nu\bar{\nu} + 4$  jets using `MadGraph5_aMC@NLO` [10] and `MadAnalysis` [13]. For the specific settings of cuts on the external particles to distinguish the final states and to reduce background we refer to Ref. [3]. If at the same time the Higgs to gauge boson couplings and the total width  $\Gamma_H$  entering the on-shell cross section are varied such, that the on-shell cross section remains constant, the off-shell contributions develop a dependence on the Higgs width. Thus, the total number of events with an invariant mass of the four jets  $m_{4j} > 130$  GeV can be ultimately expressed in the form [3]

$$N(r) = N_0(1 + R_1\sqrt{r} + R_2r) + N_B \quad , \quad (5)$$

where  $r = \Gamma_H/\Gamma_H^{\text{SM}}$  and  $N_0, N_B, R_1, R_2$  are constants. The linear dependence on  $r$  stems from the Higgs boson induced off-shell contributions, whereas the  $\sqrt{r}$  dependence is induced from Higgs to background interference terms.

We show the normalised event rates  $N(r)/N(1)$  for a cms energy of  $\sqrt{s} = 1$  TeV in Fig. 4, where we add in addition the exclusion range of  $r$  and thus  $\Gamma_H$  for different integrated luminosities, which is based on the 95% uncertainty band following a simplistic Bayesian approach [3]. The sensitivity to  $r$  for large  $\sqrt{s}$  is even for quite high statistics lowered by the interference terms of Higgs induced diagrams and background diagrams, which lead to a minimum of  $N(r)$  in the vicinity of one. A similar reduced sensitivity around  $r \sim 1$  applies to the LHC analysis [3]. At an  $e^+e^-$  collider Higgsstrahlung induced processes are less affected by the negative interference, but often limited by low statistics.

### 3 Signal-background interference in $H \rightarrow \gamma\gamma$

Subsequently we discuss the signal-background interference in  $H \rightarrow \gamma\gamma$  at an  $e^+e^-$  collider for the Higgsstrahlung process and comment on the differences for the vector-boson fusion process. As pointed out in Ref. [14] for the gluon fusion Higgs production channel at the LHC

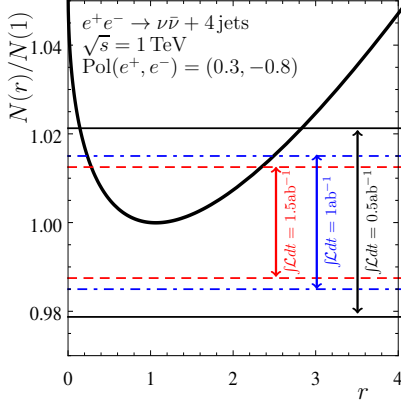


Figure 4: Normalised event rates  $N(r)/N(1)$  as a function of  $r$  for  $e^+e^- \rightarrow \nu\bar{\nu} + 4\text{jets}$  for  $\sqrt{s} = 1 \text{ TeV}$  with 95% uncertainty bands for different integrated luminosities.

the mass peak in  $H \rightarrow \gamma\gamma$  is shifted from interference with background, which is meanwhile worked out in more detail and at higher orders [15]. A similar shift is also expected at an  $e^+e^-$  collider as we demonstrate below. Again we performed a calculation using **FeynArts** and **FormCalc** [9] at lowest order and implemented the Higgs-photon-photon interaction as effective vertex given by [14]

$$\begin{array}{c} \gamma \\ | \\ \text{---} \bullet \text{---} \\ | \\ \gamma \end{array} \quad H \text{---} = \frac{i\sqrt{2}G_F}{4\pi} m_{\gamma\gamma}^2 \left[ F_1(4m_W^2/m_{\gamma\gamma}^2) + \sum_{f=t,b,c,\tau} N_f e_f^2 F_{1/2}(4m_f^2/m_{\gamma\gamma}^2) \right] \quad , \quad (6)$$

where  $m_{\gamma\gamma}^2$  determines the invariant mass of the photons,  $N_f = 3(1)$  for quarks (leptons) with electric charge  $e_f$  and mass  $m_f$  and  $G_F$  denotes the Fermi constant. The functions  $F_1$  and  $F_{1/2}$  can be found in Ref. [14]. Making use of the effective vertex in Eq. (6) example Feynman diagrams for the signal and the background for  $e^+e^- (\rightarrow ZH) \rightarrow Z\gamma\gamma$  are shown in Fig. 5.

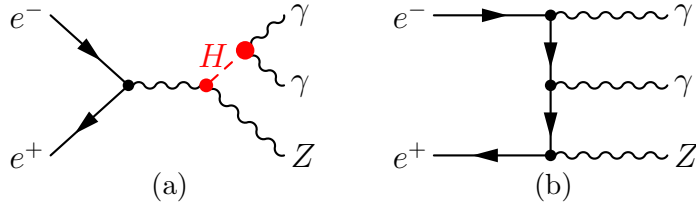


Figure 5: Feynman diagrams for  $e^+e^- \rightarrow Z\gamma\gamma$  classified as (a) signal and (b) background.

We start with the discussion of the background for both production processes. In order to avoid infrared singularities we apply a cut on the photon energies of  $E_\gamma > 20 \text{ GeV}$  and to take care of collinear singularities we cut on the photon pseudorapidity  $|\eta_\gamma| < 2$ . Similar cuts were already applied in previous works [16, 17]. A cut on the transverse momentum  $p_T$  leads to similar findings. For  $e^+e^- \rightarrow Z\gamma\gamma$  Fig. 6 (a-c) show the cross section as a function of the invariant mass of the two outgoing photons  $m_{\gamma\gamma}$  in fb/GeV for cms energies  $\sqrt{s} = 250, 350, 500 \text{ GeV}$ . The integrated inclusive cross section is in accordance to Ref. [17] and a calculation with **CalcHEP** [18]. The differential cross section is reproduced with the help of **MadGraph5\_aMC@NLO** [10]. In case of  $e^+e^- \rightarrow ZH$  the Higgs is likely to have a non-vanishing transverse momenta, which leads to two photons with a small opening angle. Thus,

the background and therefore also the signal-background interference is lowered, when the maximal value of  $|\eta_\gamma|$  is increased and/or the opening angle between the two photons is restricted to small values.

The background around  $m_{\gamma\gamma} \approx m_H$  follows a rather smooth behaviour, which allows its subtraction by a side-band analysis and therefore the determination of the mass peak and its shift due to the signal-background interference. The maximum in  $d\sigma_B^{Z\gamma\gamma}/dm_{\gamma\gamma}$  close to  $m_{\gamma\gamma} \sim m_H$  stems from the applied cuts and shifts by lowering/increasing the minimal photon energy  $E_\gamma$ . Cross sections for the pure background contribution, named  $\sigma_B$ , and the signal contribution  $\sigma_S$  can be taken from Tab. 2. The contributions of the interference term  $\sigma_I$  to the inclusive cross section are negligible. All contributions scale equally with the polarisation of the initial state in case of  $e^+e^- (\rightarrow ZH) \rightarrow Z\gamma\gamma$ , thus the relative ratio between signal and background is independent of the polarisation. The same applies to  $e^+e^- (\rightarrow \nu\bar{\nu}H) \rightarrow \nu\bar{\nu}\gamma\gamma$  for large  $\sqrt{s}$ , where the  $Z \rightarrow \nu\bar{\nu}$  induced final states are of minor relevance.

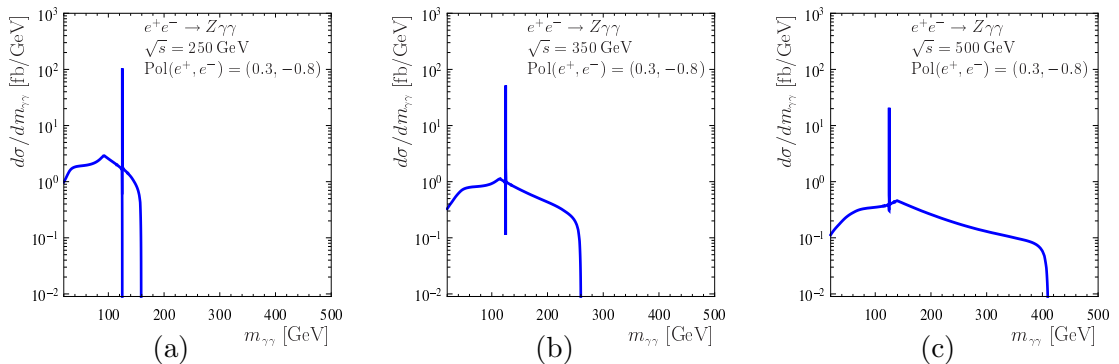


Figure 6:  $d\sigma/dm_{\gamma\gamma}$  in fb/GeV as a function of  $m_{\gamma\gamma}$  in GeV for  $e^+e^- \rightarrow Z\gamma\gamma$  with cms energies (a-c)  $\sqrt{s} = 250, 350, 500$  GeV for  $\text{Pol}(e^+, e^-) = (0.3, -0.8)$  and  $E_\gamma > 20$  GeV,  $|\eta_\gamma| < 2$ .

$\sqrt{s}$	$\sigma_B^{Z\gamma\gamma}$	$\sigma_{B,\text{cut}}^{Z\gamma\gamma}$	$\sigma_S^{Z\gamma\gamma}$
250 GeV	260 fb	51.10 fb	0.89 fb
300 GeV	194 fb	38.88 fb	0.67 fb
350 GeV	152 fb	29.76 fb	0.48 fb
500 GeV	87 fb	11.90 fb	0.21 fb
1 TeV	30 fb	1.75 fb	0.05 fb

Table 2: Inclusive cross sections for  $e^+e^- (\rightarrow ZH) \rightarrow Z\gamma\gamma$  separated in signal and background contributions for  $\text{Pol}(e^+, e^-) = (0.3, -0.8)$  and for different cms energies  $\sqrt{s}$ . The background in the “signal region” is defined by  $\sigma_{B,\text{cut}} = \sigma_B(110 \text{ GeV}, 140 \text{ GeV})$  in the notation of Eq. (4).

In Fig. 7 we focus on the signal contribution  $\sigma_S$ , being the process  $e^+e^- \rightarrow ZH \rightarrow Z\gamma\gamma$ , and the signal-background interference  $\sigma_{S+I}$  in the window around  $m_{\gamma\gamma} \approx 125$  GeV using the described cuts and polarisation of the initial state. The photon energies are usually smeared by detector effects, which thus need to be discussed by the experimental collaborations. We convoluted with a Gaussian function with a Gaussian width of  $\hat{\sigma} = 1$  GeV. The resulting cross sections are denoted  $\sigma^G$ . This convolution lowers the height of  $\sigma_S \rightarrow \sigma_S^G$  and  $\sigma_{S+I} \rightarrow \sigma_{S+I}^G$ , but broadens the peaks accordingly. The mass shift is therefore enlarged. For the case of Fig. 7 the smeared mass peaks are shown in Fig. 8. In case  $Z$  boson decays are considered in addition, more background diagrams get involved and thus affect the shift of the mass peak.

To quantify the shift we closely follow Ref. [14]. Supposing that the experimental collaborations reduce the background by a suitable side-band analysis, we are left with the shifted



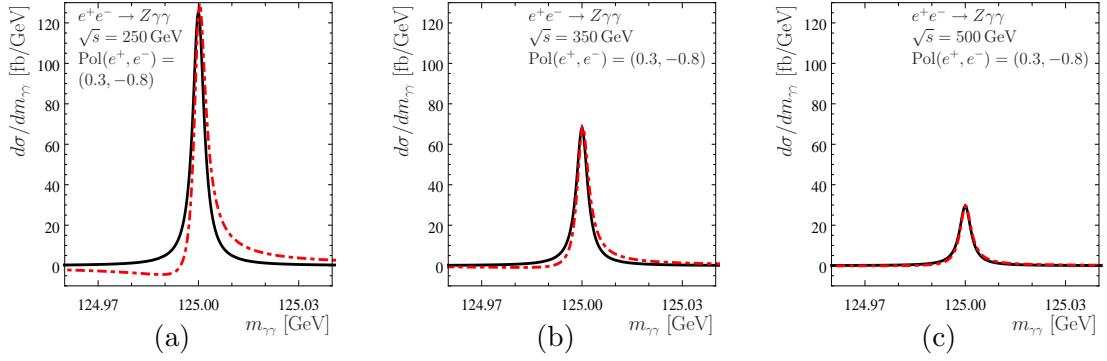


Figure 7:  $d\sigma_S/dm_{\gamma\gamma}$  (black, solid) and  $\sigma_{S+I}/dm_{\gamma\gamma}$  (red, dot-dashed) in fb/GeV as a function of  $m_{\gamma\gamma}$  in GeV for  $e^+e^- \rightarrow Z\gamma\gamma$  for (a-c)  $\sqrt{s} = 250, 350, 500$  GeV.

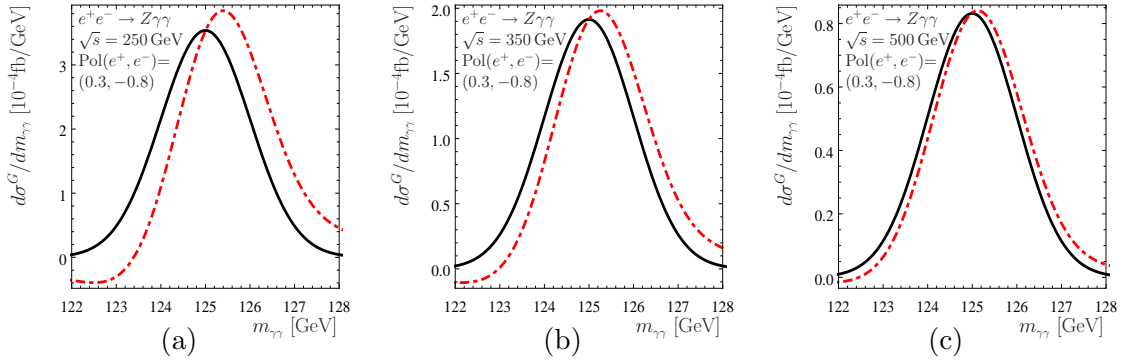


Figure 8: Smeared  $d\sigma_S^G/dm_{\gamma\gamma}$  (black, solid) and  $\sigma_{S+I}^G/dm_{\gamma\gamma}$  (red, dot-dashed) in fb/GeV as a function of  $m_{\gamma\gamma}$  in GeV for  $e^+e^- \rightarrow Z\gamma\gamma$  with  $\hat{\sigma} = 1$  GeV for (a-c)  $\sqrt{s} = 250, 350, 500$  GeV.

signal event rate. To determine the mass peak a simplistic way is given by the mean  $\langle m_{\gamma\gamma} \rangle$  within the interval  $[m_p - \delta_\gamma, m_p + \delta_\gamma]$ , where  $m_p$  is the actual mass peak of the distribution and  $\delta_\gamma$  is given by the experiment. Then we define [14]

$$\langle m_{\gamma\gamma} \rangle_{\delta, X} = \frac{1}{N_{\delta, X}} \int_{m_p - \delta}^{m_p + \delta} dm_{\gamma\gamma} m_{\gamma\gamma} \frac{d\sigma_X^G}{dm_{\gamma\gamma}} \quad \text{with} \quad N_{\delta, X} = \int_{m_p - \delta}^{m_p + \delta} dm_{\gamma\gamma} \frac{d\sigma_X^G}{dm_{\gamma\gamma}} \quad . \quad (7)$$

A theoretical measure of the shift is given by

$$\Delta m_{\gamma\gamma} = \langle m_{\gamma\gamma} \rangle_{\delta_\gamma, S+I} - \langle m_{\gamma\gamma} \rangle_{\delta_\gamma, S} \quad . \quad (8)$$

We note that the experiments can access only  $\langle m_{\gamma\gamma} \rangle_{\delta_\gamma, S+I}$ . To obtain a normalization of the shift, either other production or decay channels have to be considered to obtain the actual Higgs mass or alternatively different kinematic regions in  $H \rightarrow \gamma\gamma$  allow for the observation of different shifts. The latter method can e.g. be understood by applying different cuts on the transverse momentum  $p_T$  or the angle between the two photons. A detailed detector simulation is on order, which is beyond the scope of our considerations. We instead try to quantify the effect using the theoretical measure  $\Delta m_{\gamma\gamma}$  as a function of  $\delta_\gamma$  and present  $\Delta m_{\gamma\gamma}$  for two Gaussian widths  $\hat{\sigma} = 1$  and  $1.5$  GeV in Fig. 9 (a) for different cms energies.

The large background for  $e^+e^- \rightarrow Z\gamma\gamma$  at low cms energies  $\sqrt{s}$  induces a sizeable shift  $\Delta m_{\gamma\gamma}$ . For low values of  $\delta_\gamma$  the mass shift  $\Delta m_{\gamma\gamma}$  corresponds to the actual difference between the two peaks of the distributions after Gaussian smearing as given in Fig. 8. For large values of  $\delta_\gamma > 2\hat{\sigma}$  the mass shift  $\Delta m_{\gamma\gamma}$  increases linearly, since more of the tail of the signal-background

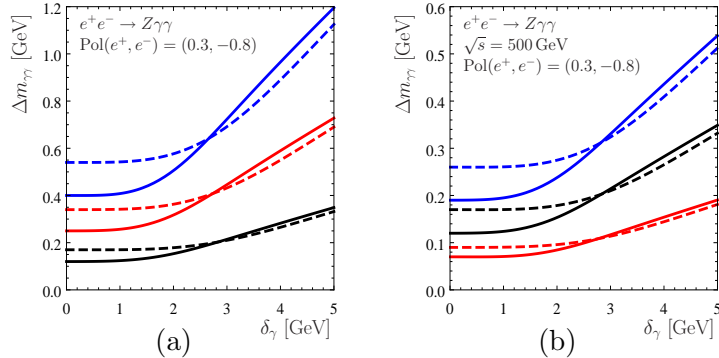


Figure 9: (a)  $\Delta m_{\gamma\gamma}$  in GeV as a function of  $\delta_\gamma$  in GeV for  $e^+e^- \rightarrow Z\gamma\gamma$  with cms energies  $\sqrt{s} = 250$  GeV (blue), 350 GeV (red) and 500 GeV (black); (b)  $\Delta m_{\gamma\gamma}$  in GeV as a function of  $\delta_\gamma$  in GeV for  $e^+e^- \rightarrow Z\gamma\gamma$  for  $\sqrt{s} = 500$  GeV with  $\Gamma_H = 1$  MeV (red), 4.07 MeV (black) and 15 MeV (blue). Both figures include two Gaussian widths  $\hat{\sigma} = 1$  GeV (solid) and  $\hat{\sigma} = 1.5$  GeV (dashed).

interference is included. To show the dependence of the shift on the width  $\Gamma_H$  of the Higgs boson, we perform a similar analysis as in Section 2 and change the Higgs width in combination with a rescaling of the  $HVV$  couplings to leave the inclusive on-shell Higgs cross section constant. For simplicity we rescale all  $HVV$  couplings including the loop-induced Higgs boson to photons coupling equally. Apart from the SM value we pick the Higgs widths  $\Gamma_H = 1$  MeV and  $\Gamma_H = 15$  MeV. Fig. 9 (b) shows  $\Delta m_{\gamma\gamma}$  as a function of  $\delta_\gamma$  for different values of  $\Gamma_H$  for  $\sqrt{s} = 500$  GeV. The mass shift, being of the order of  $\mathcal{O}(100$  MeV), shows a clear dependence on the Higgs width. Similar findings and shifts in the invariant mass peak of the two photons can be obtained for the vector-boson fusion process, but we leave a detailed presentation to future work.

## 4 Conclusions

We quantified the shift of the invariant mass peak in Higgs boson to photon decays  $H \rightarrow \gamma\gamma$  induced by the signal-background interference at an  $e^+e^-$  collider for the Higgsstrahlung process  $e^+e^- \rightarrow Z\gamma\gamma$ . The observed mass shift is strongly dependent on detector effects, but expected to be in the range of  $\mathcal{O}(100$  MeV). Similar effects occur for the vector-boson fusion induced Higgs production process and both allow to access the Higgs width. Similarly we quantified off-shell contributions in  $H \rightarrow VV^{(*)}$  with  $V \in \{Z, W\}$  for both production processes for different polarisations and cms energies. At larger cms energies  $\sqrt{s} > 500$  GeV they contribute  $\mathcal{O}(10\%)$  to the total Higgs boson induced cross section. Whereas the  $Z$  recoil method at low cms energies is thus safe from off-shell contributions, the off-shell region allows to extract the Higgs boson to gauge boson couplings in different kinematical regimes and thus to test the electroweak symmetry breaking mechanism. The determination of the Higgs width from a combination of on- and off-shell measurements in Higgs boson decays to heavy gauge bosons – besides relying on strong theoretical assumptions – is mainly limited by the negative signal-background interference term in the off-shell region.

## Acknowledgments

The author acknowledges support by “Deutsche Forschungsgemeinschaft” through the SFB 676 “Particles, Strings and the Early Universe”.

## References

- [1] G. Aad *et al.* [ATLAS Collaboration], Phys. Lett. B **716** (2012) 1 [arXiv:1207.7214].
- [2] S. Chatrchyan *et al.* [CMS Collaboration], Phys. Lett. B **716** (2012) 30 [arXiv:1207.7235].
- [3] S. Liebler, G. Moortgat-Pick and G. Weiglein, arXiv:1502.07970.
- [4] S. Dittmaier *et al.* [LHC Higgs Cross Section Working Group Coll.], arXiv:1101.0593.  
S. Dittmaier *et al.* [LHC Higgs Cross Section Working Group Coll.], arXiv:1201.3084.  
S. Heinemeyer *et al.* [LHC Higgs Cross Section Working Group Coll.], arXiv:1307.1347.
- [5] N. Kauer and G. Passarino, JHEP **1208** (2012) 116 [arXiv:1206.4803]. N. Kauer, Mod. Phys. Lett. A **28** (2013) 1330015 [arXiv:1305.2092]. N. Kauer, JHEP **1312** (2013) 082 [arXiv:1310.7011]. N. Kauer, arXiv:1502.02581.
- [6] F. Caola and K. Melnikov, Phys. Rev. D **88** (2013) 054024 [arXiv:1307.4935].  
J. M. Campbell, R. K. Ellis and C. Williams, JHEP **1404** (2014) 060 [arXiv:1311.3589].  
J. M. Campbell, R. K. Ellis and C. Williams, Phys. Rev. D **89** (2014) 053011 [arXiv:1312.1628].  
M. Chen, T. Cheng, J. S. Gainer, A. Korytov, K. T. Matchev, P. Milenovic, G. Mitselmakher and M. Park *et al.*, Phys. Rev. D **89** (2014) 034002 [arXiv:1310.1397].  
I. Moutl and I. W. Stewart, JHEP **1409** (2014) 129 [arXiv:1405.5534].  
J. M. Campbell, R. K. Ellis and C. Williams, PoS LL **2014** (2014) 008 [arXiv:1408.1723].  
J. M. Campbell, R. K. Ellis, E. Furlan and R. Rötsch, Phys. Rev. D **90** (2014) 9, 093008 [arXiv:1409.1897].  
J. M. Campbell and R. K. Ellis, arXiv:1502.02990.
- [7] C. Englert and M. Spannowsky, Phys. Rev. D **90** (2014) 053003 [arXiv:1405.0285].  
M. Ghezzi, G. Passarino and S. Uccirati, PoS LL **2014** (2014) 072 [arXiv:1405.1925].  
C. Englert, Y. Soreq and M. Spannowsky, arXiv:1410.5440. H. E. Logan, arXiv:1412.7577.
- [8] CMS Collaboration [CMS Collaboration], CMS-PAS-HIG-14-002. V. Khachatryan *et al.* [CMS Collaboration], Phys. Lett. B **736** (2014) 64 [arXiv:1405.3455]. ATLAS collaboration [ATLAS collaboration], ATLAS-CONF-2014-042.
- [9] T. Hahn and M. Perez-Victoria, Comput. Phys. Commun. **118** (1999) 153 [hep-ph/9807565]. T. Hahn, Comput. Phys. Commun. **140** (2001) 418 [hep-ph/0012260].
- [10] J. Alwall, M. Herquet, F. Maltoni, O. Mattelaer and T. Stelzer, JHEP **1106** (2011) 128 [arXiv:1106.0522].
- [11] E. Maina, arXiv:1501.02139. N. Kauer and C. O'Brien, arXiv:1502.04113. J. Baglio, J. Bellm, F. Campanario, B. Feigl, J. Frank, T. Figy, M. Kerner and L. D. Ninh *et al.*, arXiv:1404.3940. C. Englert, I. Low and M. Spannowsky, arXiv:1502.04678.
- [12] H. Li *et al.* [ILD Design Study Group Collaboration], arXiv:1202.1439. A. Miyamoto, arXiv:1311.2248. Talks by T. Barklow and S. Watanuki at LCWS 2014, Belgrade, Serbia, <http://agenda.linearcollider.org/event/6389>
- [13] E. Conte, B. Fuks and G. Serret, Comput. Phys. Commun. **184** (2013) 222 [arXiv:1206.1599].
- [14] S. P. Martin, Phys. Rev. D **86** (2012) 073016 [arXiv:1208.1533].
- [15] D. de Florian, N. Fianza, R. J. Hernández-Pinto, J. Mazzitelli, Y. Rotstein Habarnau and G. F. R. Sborlini, Eur. Phys. J. C **73** (2013) 2387 [arXiv:1303.1397]. S. P. Martin, Phys. Rev. D **88** (2013) 1, 013004 [arXiv:1303.3342]. L. J. Dixon and Y. Li, Phys. Rev. Lett. **111** (2013) 111802 [arXiv:1305.3854].
- [16] V. D. Barger, T. Han and R. J. N. Phillips, Phys. Rev. D **39** (1989) 146.
- [17] W. J. Stirling and A. Werthenbach, Eur. Phys. J. C **14** (2000) 103 [hep-ph/9903315].
- [18] A. Belyaev, N. D. Christensen and A. Pukhov, Comput. Phys. Commun. **184** (2013) 1729 [arXiv:1207.6082].